



## Article

# Design of an Active Damping System for Vibration Control of Wind Turbine Towers

Hao Bai , Younes Aoues , Jean-Marc Cherfils and Didier Lemosse

Laboratory of Mechanics of Normandy (LMN), INSA Rouen Normandie, 76000 Rouen, France; younes.aoues@insa-rouen.fr (Y.A.); jean-marc.cherfils@insa-rouen.fr (J.-M.C.); didier.lemosse@insa-rouen.fr (D.L.)  
\* Correspondence: hao.bai@insa-rouen.fr; Tel.: +33-2-32-95-99-79

**Abstract:** The vibration of wind turbine towers is relevant to the reliability of the wind turbine structure and the quality of power production. It produces both ultimate loads and fatigue loads threatening structural safety. This paper aims to reduce vibration in wind turbine towers using an active damper named the twin rotor damper (TRD). A single degree of freedom (SDOF) oscillator with the TRD is used to approximate the response of wind turbines under a unidirectional gusty wind with loss of the electrical network. The coincidence between the wind gust and the grid loss is studied to involve the maximum loading on the structure. The performance of the proposed damping system under the maximum loading is then evaluated on the state-of-the-art wind turbine NREL 5 MW. The effectiveness of the TRD is compared to a passive tuned mass damper (TMD) designed with similar requirements. The numerical results reveal that, at the 1st natural mode, the TRD outperforms the passive TMD by three to six times. Moreover, the results show that the TRD is effective in reducing ultimate loads on wind turbine towers.



**Citation:** Bai, H.; Aoues, Y.; Cherfils, J.-M.; Lemosse, D. Design of an Active Damping System for Vibration Control of Wind Turbine Towers. *Infrastructures* **2021**, *6*, 162. <https://doi.org/10.3390/infrastructures6110162>

Academic Editors: José Campos e Matos, Hélder S. Sousa, Alfred Strauss and Emilio Bastidas-Arteaga

Received: 8 September 2021  
Accepted: 4 November 2021  
Published: 11 November 2021

**Publisher's Note:** MDPI stays neutral with regard to jurisdictional claims in published maps and institutional affiliations.



**Copyright:** © 2021 by the authors. Licensee MDPI, Basel, Switzerland. This article is an open access article distributed under the terms and conditions of the Creative Commons Attribution (CC BY) license (<https://creativecommons.org/licenses/by/4.0/>).

**Keywords:** wind turbine tower; vibration control; active damping system; twin rotor damper; ultimate analysis

## 1. Introduction

With the fast-growing wind energy industry, the requirement for a reliable wind turbine tower is critical in terms of the structural safety and power production. Since the wind resource is more stable (i.e., less wind turbulence) and more sustainable (i.e., more convertible wind resource) in high altitude (generally speaking, higher than 100 m), the wind turbines are growing taller to extract more energy. However, just like all the other technologies in this world, there is always a trade-off—the quest for higher and larger turbines comes with its fair share of engineering challenges.

To give an illustration, taller wind turbine towers suffer from highly intensive loads induced directly by the airflow and indirectly from the nacelle and the blades. The vibrations and ultimate loads transferred to the tower reduce its service life and involve many other problems such as cracks due to the fatigue damage. To overcome this mechanical engineering challenge, the two foremost used approaches are modified controller methods and damper based methods. The former is mainly based on Pitch Angle Control (PAC) that controls the blades' pitch angle to counterbalance the vibrations on the wind turbine tower [1–3]. Due to the limited rotation speed of the pitch angle, this method usually has a slow response. However, it enhances the vibration control with minimum extra cost since there is no need for additional equipment. On the contrary, the damper-based methods are more effective in reducing vibrations as they embed a specifically designed damping system inside the wind turbine. Absorber systems are widely used in civil engineering structures to reduce vibration responses [4–6]. However, some of these methods are of significant cost.

The embedded damping system can be mainly categorized into three types: passive, semi-active, and active. One of the famous damping systems is Tuned Mass Damper

(TMD), which is employed in different structures such as bridges and tall buildings [7], foot-bridges [8] and submerged floating tunnel [9]. As for wind turbine structures, Si et al. [10] have applied TMD on spar platforms for offshore wind turbines. It showed that the performance of TMD depends mainly on its mechanical properties, namely the spring coefficient and the damping ratio. The TMD with a large spring and damping ratio offered a considerable load reduction when the turbine is working below rated or in low-frequency resonant motion. In contrast, the TMD with a small spring coefficient contributed much to load reduction when the turbine is working above the rated condition. Tong et al. [11] proposed to use a bidirectional tuned liquid column damper (BTLCD) to reduce the tower loads. The numerical simulations revealed that BTLCD can reduce loads by up to 27%. Stewart and Lackner [12] have proposed a set of optimum TMDs by creating a limited degree-of-freedom model for both onshore wind turbines and offshore ones with a barge, monopile, spar buoy, or tension-leg platform. A load reduction by up to 20% is achieved for the various TMD configurations. Despite all these achievements, the passive dampers have some downsides when applied to wind turbines. Firstly, based on its principle, passive dampers need to be massive in order to deliver an effective damping force. This explains why the passive dampers nowadays are mainly implemented on the supporting platform of offshore wind turbines [13–16]. Secondly, the passive dampers are tuned to a single frequency. Consequently, they are only effective over a narrow-band of frequencies. It is hard to tune the passive dampers to reduce vibrations for rotor frequency (1P) and blade passing frequency (3P).

To overcome such issues, an active damper is an effective solution. Fitzgerald and Basu [17] combined a TMD with a control algorithm through a cable to reduce in-plane vibrations for wind turbine blades. Coudurier et al. [18] proposed a control strategy to improve the effectiveness of tuned liquid column dampers (TLCD) for offshore wind turbines. Some recent researches [19–22] proposed to reduce the vibrations on wind turbine towers by operating the pitch angles of the blades. Since the power production of wind turbines relies on the wind source captured by the blades, using the pitch control to damp the wind tower vibrations may lead to a loss in the power production. Therefore, Gambier [23] has investigated such a problem by using multi-objective optimization in order to seek an optimal balance between the pitch control and the active tower damping control. Active dampers have significant advantages over passive dampers in damping a broader band of frequencies and more control availabilities [24]. However, an external power supply is mandatory, which limits the application of those active dampers. Moreover, the complexity of the active damper's structure and control system also leads to reducing their maintainability and reliability.

Recently, Scheller [25] proposed a new active damper named the twin rotor damper (TRD) for damping structural vibrations. Unlike other active dampers, TRD generates the damping force from rotating control masses instead of accelerating and decelerating control masses [26]. This makes TRD more power-efficient and opens the possibility of implementing an active damper in limited space such as the inner space of a wind turbine tower. To the best of our knowledge, an active damping system inside the wind turbine tower with such a device has not been discussed yet. In addition, most current research focuses on turbulent wind conditions [10–12,17,21,27]. In this paper, we study the feasibility of using the TRD for vibration control of wind turbine towers. A theoretical prototype of the damping system (i.e., the damper and the associated control algorithm) is proposed for a baseline wind turbine. An idealistic wind gust is involved to evaluate the effectiveness of the proposed system in reducing peak-to-peak amplitude.

The main contributions of this paper include:

- A grid search on the timing of an internal or external electrical system fault combined to gusty wind conditions with respect to IEC61400 standards;
- Theoretical design of an active damping system including the TRD and a control algorithm to reduce the vibrations of wind turbine towers;

- Evaluation of the proposed damping system in an extreme load event triggered by the loss of electrical network connection while the turbine is producing power;
- Investigations and discussions on the use of TRD for damping wind turbine vibrations; a comparison between TRD and other types of damping system used in the wind industry.

The rest of the paper is organized as follows: a brief presentation of the TRD is given in Section 2; the design of an active damping system using the TRD is presented in Section 3; numerical simulations are used to demonstrate the efficiency of the proposed damping system in Section 4; conclusions and outlooks are presented in Section 5.

## 2. Twin Rotor Damper (TRD)

### 2.1. Theory and Layout

Twin rotor damper (TRD) is a type of active damper invented by U. Starossek and patented by Soletanche Freyssinet [28]. It is an active damper based on the centrifugal forces produced by two counter-rotating control masses about parallel axes. Figure 1 illustrates the fundamental layout of TRD in which two control masses of  $\frac{m_c}{2}$  are hinged eccentrically to two actuators. The mass of the two rods that connect the control masses to the axes of rotation is omitted. The length of these rods, denoted as  $r$ , is named as the radius of TRD. The angular position  $\varphi(t)$  determines the motion of two rotors (i.e., the control masses with mass-less rods).

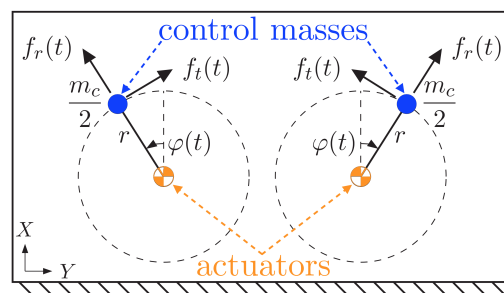


Figure 1. Layout of twin rotor damper (TRD) [29].

The motion of a single rotor generates a radial force:

$$f_r(t) = \frac{1}{2}m_c r \dot{\varphi}^2(t) \tag{1}$$

and a tangential force which appears when the control mass is accelerated:

$$f_t(t) = \frac{1}{2}m_c r \ddot{\varphi}(t). \tag{2}$$

If the angular positions  $\varphi(t)$  of the two rotors are the same, the Y-components of the radial forces  $f_r(t)$  and that of the tangential forces  $f_t(t)$  cancel each other, while the X-components are superimposed. Therefore, the resultant force  $f_{TRD}$  of two rotors is:

$$f_{TRD}(t) = m_c r \left[ \dot{\varphi}^2(t) \cos \varphi(t) + \ddot{\varphi}(t) \sin \varphi(t) \right] \tag{3}$$

On the right side of Equation (3), the first term corresponds to the radial force  $f_r(t)$ , and the second one is the tangential force  $f_t(t)$ . The use of these two forces determines the TRD working mode.

In continuous rotation mode, both rotors are driven by a steady angular velocity  $\dot{\varphi}$ , the control force is then majorly composed by the radial force  $f_r(t)$  since the term of tangential force vanishes. It should be noted that Bäumer et al. [30] proposed an alternative swinging mode of operation which mainly involves tangential forces  $f_t(t)$  by continuously accelerating/decelerating the two rotors.

This work focuses on the continuous rotation mode and the definition of a target angular velocity  $\dot{\varphi}_t$  for the TRD. When the masses reach that steady velocity, the resultant force then reads:

$$f_{TRD}(t) = m_c r \dot{\varphi}_t^2 \cos \varphi_t(t). \tag{4}$$

This force can be set to counteract any single degree of freedom (SDOF) oscillator moving in its natural modes. In the next section, we will describe such an oscillator which could stand for a wind turbine induced by unidirectional loading. Then the control force  $f_{TRD}(t)$  will be applied to the tower-top of a numerical model of wind turbine facing gusty wind in order to control vibrations on the natural frequency.

### 2.2. Single Degree of Freedom (SDOF) Oscillator

A single degree of freedom (SDOF) oscillator, equipped with a TRD, is described on Figure 2. The motion equation of this oscillator is:

$$(m + m_c)\ddot{x}(t) + c\dot{x}(t) + kx(t) = f_e(t) + f_{TRD}(t). \tag{5}$$

On the left-hand side of Equation (5), the terms stand respectively for the inertial force of the system (including the control masses), the damping force and the restoring spring force. The oscillating system is characterized by the stiffness  $k$ , the damping coefficient  $c$ , and the total mass  $m + m_c$ , where  $m$  stands for the mass of oscillator and  $m_c$  for the TRD mass. On the right-hand side, the SDOF is excited by an external loading  $f_e(t)$  and should be stabilized by the force generated by the TRD  $f_{TRD}(t)$ .

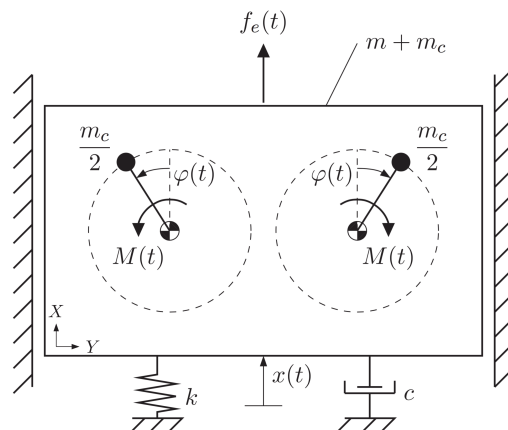


Figure 2. TRD on a single degree of freedom (SDOF) oscillator [30].

Dividing Equation (5) by  $(m + m_c)$  yields:

$$\ddot{x}(t) + 2\zeta\omega_n\dot{x}(t) + \omega_n^2x(t) = F_e(t) + F_{TRD}(t). \tag{6}$$

where,  $F_e(t) = \frac{f_e(t)}{m+m_c}$  excitation force normalized by  $m + m_c$   
 $F_{TRD}(t) = \frac{f_{TRD}(t)}{m+m_c}$  TRD control force normalized by  $m + m_c$   
 $\mu_c = \frac{m_c}{m+m_c}$  control mass ratio  
 $\omega_n = \sqrt{\frac{k}{m+m_c}}$  natural angular frequency of the system  
 $\zeta = \frac{c}{2} \sqrt{\frac{1}{k(m+m_c)}}$  damping ratio of the system.

Assuming that the damping ratio of the system  $\zeta$  is zero, Equation (6) can be simplified to:

$$\ddot{x}(t) + \omega_n^2x(t) = F_e(t) + F_{TRD}(t). \tag{7}$$

This normalized equation of motion is converted to state-space equations in the following section in order to design an appropriate control algorithm with feedback.

Coming from the motion equation of a single rotor of the TRD, the moment  $M(t)$  provided by one actuator is:

$$M(t) = J\ddot{\varphi}(t) - \frac{1}{2}m_c r \ddot{x}(t) \sin \varphi(t). \tag{8}$$

On the left side of Equation (8),  $M(t)$  is the moment created by one actuator. On the right side,  $J$  is the moment inertia of a single rotor and  $\ddot{\varphi}(t)$  is the angular acceleration of a rotor, the second term is the moment induced by the translational acceleration of the SDOF oscillator.

In the real-world application, the moment  $M(t)$  depends on the properties of the used actuator such as the response time, the efficiency, and so forth. To avoid these drawbacks and to simplify the analysis in this work, we decided to directly control the angular position  $\varphi(t)$  of the rotor instead of the moment  $M(t)$ . For more information about Equation (5), Equation (8) and the generation of the control force, see [25,29].

### 2.3. Phasing the TRD with the SDOF Oscillator

#### 2.3.1. Theory

In order to use the TRD to reduce the vibrations of the wind turbine tower, it is necessary to design a control algorithm for the oscillating motion. In control engineering, state-space equations are conventionally used to describe a dynamic system [31]. To achieve a state-space representation of Equation (7), a state vector must be first defined. It should contain all variables that are needed to describe the dynamic behavior of the system such that:

$$\mathbf{x}_s(t) = \begin{bmatrix} x(t) \\ \dot{x}(t) \end{bmatrix}, \tag{9}$$

where  $\mathbf{x}_s(t)$  is the state vector,  $x(t)$  and  $\dot{x}(t)$  are the state variables representing the displacement and the velocity of SDOF oscillator, respectively.

Similarly, the TRD part can be described by a state vector  $\boldsymbol{\varphi}_s(t)$  like:

$$\boldsymbol{\varphi}_s(t) = \begin{bmatrix} \varphi(t) \\ \dot{\varphi}(t) \end{bmatrix}, \tag{10}$$

where  $\varphi(t)$  and  $\dot{\varphi}(t)$  represent the actual angular position and velocity of the TRD, respectively. Likewise, the TRD target state  $\boldsymbol{\varphi}_t(t)$  is defined by:

$$\boldsymbol{\varphi}_t(t) = \begin{bmatrix} \varphi_t(t) \\ \dot{\varphi}_t(t) \end{bmatrix}, \tag{11}$$

where  $\varphi_t(t)$  and  $\dot{\varphi}_t(t)$  represent the target angular position and velocity of the TRD, respectively.

Inserting the state vector (Equation (9)) into the equation of motion (Equation (7)) and solving in a Linear Time-Invariant (LTI) system [32] yields the state-space equations for SDOF oscillator:

$$\dot{\mathbf{x}}_s(t) = \mathbf{A}\mathbf{x}_s(t) + \mathbf{B}[F_e(t) + F_{TRD}(t)] \tag{12}$$

$$x(t) = \mathbf{C}\mathbf{x}_s(t), \tag{13}$$

where Equation (12) is called state equation for the system, Equation (13) is called output equation for the system,  $\mathbf{x}_s(t)$  is the state vector given in Equation (9),  $x(t)$  is the output signal,  $[F_e(t) + F_{TRD}(t)]$  is the disturbance and the control signal, respectively.  $\mathbf{A}$  is the state matrix (or system matrix) defined by:

$$\mathbf{A} = \begin{bmatrix} 0 & 1 \\ -\omega_n^2 & 0 \end{bmatrix} \tag{14}$$

$B$  is the input vector (or control vector):

$$B = \begin{bmatrix} 0 \\ 1 \end{bmatrix} \tag{15}$$

$C$  is the output vector:

$$C = [1 \ 0]. \tag{16}$$

### 2.3.2. Observer Design

Supposing that an estimate of the state vector  $x_s(t)$  is observed and denoted as  $\hat{x}_s(t)$ , thus the state-space equations for this estimate are:

$$\dot{\hat{x}}_s(t) = A\hat{x}_s(t) + B[F_{TRD}(t) + F_e(t)] \tag{17}$$

$$\hat{x}(t) = C\hat{x}_s(t). \tag{18}$$

Subtracting Equation (18) from Equation (13) shows up the error of the displacement:

$$x(t) - \hat{x}(t) = C[x_s(t) - \hat{x}_s(t)]. \tag{19}$$

Based on the principle of feedback control [33], the estimated model (Equation (17)) can be corrected continuously in time domain using the error of displacement (Equation (19)) as feedback, that is,

$$\dot{\hat{x}}_s(t) = A\hat{x}_s(t) + B[F_{TRD}(t) + F_e(t)] + LC[x_s(t) - \hat{x}_s(t)], \tag{20}$$

where  $L$  is a feedback gain vector of shape  $[l_1, l_2]^T$ .

Deducting Equation (20) from Equation (12) results in:

$$\dot{\hat{x}}_s(t) - \dot{\hat{x}}_s(t) = A[x_s(t) - \hat{x}_s(t)] - LC[x_s(t) - \hat{x}_s(t)], \tag{21}$$

where  $\dot{x}_s(t) - \dot{\hat{x}}_s(t)$  is the error dynamics given by the characteristic equation:

$$\det[sI - (A - LC)] = 0, \tag{22}$$

where  $s$  is the desired closed-loop poles.

To solve the Equation (22), in control engineering, a design method named pole-placement is applied [32,34]. With an appropriate proportional gain  $L$ , it is possible to force the system to have closed-loop poles at the desired locations. The value of  $L$  depends on the properties of the system.

### 2.3.3. Controller Design

To drive the TRD, a relation between the actual angular state of the rotors  $\varphi_s(t)$  and the observed state of the SDOF oscillator  $\hat{x}_s(t)$  is needed. Consequently, an additional state vector  $\psi_s(t)$  is introduced:

$$\psi_s(t) = \begin{bmatrix} \psi_1(t) \\ \psi_2(t) \end{bmatrix} = \begin{bmatrix} \arctan 2(\omega_n \hat{x}(t), \ddot{\hat{x}}(t)) \\ \arctan 2(\omega_n \hat{x}(t), \dot{\hat{x}}(t)) \end{bmatrix}, \tag{23}$$

where 2-argument arctangent function  $\arctan 2(x, y)$  is defined as:

$$\arctan 2(x, y) = \begin{cases} \arctan \frac{x}{y} & \text{for } y > 0, x > 0 \\ \arctan \frac{x}{y} + 2\pi & \text{for } y > 0, x < 0 \\ \arctan \frac{x}{y} + \pi & \text{for } y < 0 \\ \frac{\pi}{2} & \text{for } y = 0, x > 0 \\ \frac{3\pi}{2} & \text{for } y = 0, x < 0 \\ \text{undefined} & \text{for } y = 0, x = 0. \end{cases} \quad (24)$$

$\psi_s(t)$  actually describes the progress of the SDOF oscillator within one vibration cycle. Then, the differences between  $\psi_s(t)$  and the angular position  $\varphi(t)$  can be computed:

$$\begin{aligned} \alpha_1 &= \varphi(t) - \psi_1(t) \\ \alpha_2 &= \varphi(t) - \psi_2(t). \end{aligned} \quad (25)$$

$\alpha_1$  and  $\alpha_2$  describe the differences in the rotational position between the TRD and the SDOF oscillator.

For the continuous rotation mode, Bäumer et al. [35] revealed that the rotational position difference  $\alpha_2$  is nearly a constant:

$$\alpha_2 = \varphi(t) - \psi_2(t) \approx \pi. \quad (26)$$

With this information, it is possible to define the target angular position  $\varphi_t(t)$  by renaming the angular position  $\varphi(t)$  in Equation (26):

$$\varphi_t(t) = \pi + \psi_2(t). \quad (27)$$

This implies that the target angular position  $\varphi_t(t)$  is determined by the displacement  $\hat{x}(t)$  and the velocity  $\hat{\dot{x}}(t)$  of the SDOF oscillator since they are involved in the definition of  $\psi_2(t)$ , see Equation (23). As for the target angular velocity  $\dot{\varphi}_t(t)$ , Bäumer et al. [35] suggested using the natural angular frequency  $\omega_n$  of the system in order to have an optimal damping performance of the TRD, that is,

$$\dot{\varphi}_t(t) = \omega_n. \quad (28)$$

Equations (27) and (28) characterize the target state  $\varphi_t(t)$  of the TRD. By comparing it to the actual angular state  $\varphi_s(t)$ , the error in angular position  $e_1(t)$  and the error in angular velocity  $e_2(t)$  can be defined respectively:

$$\begin{aligned} e_1(t) &= \varphi_t(t) - \varphi(t) \\ e_2(t) &= \dot{\varphi}_t(t) - \dot{\varphi}(t). \end{aligned} \quad (29)$$

These are inputs for the computation of the control error  $ce_1(t)$  and  $ce_2(t)$ :

$$\begin{aligned} ce_1(t) &= e_1(t) + 2\pi n_1 \\ ce_2(t) &= e_2(t) + 2\pi n_2, \end{aligned} \quad (30)$$

where  $n_1$  and  $n_2$  are integer numbers which are to be chosen such that  $ce_1(t)$  and  $ce_2(t)$  have a value range from  $-\pi$  to  $\pi$ .

Finally, the dynamics of the TRD can be driven by a proportional-derivative controller like:

$$\dot{\varphi}_s(t) = \mathbf{G}\varphi_s(t) + \mathbf{HK} \begin{bmatrix} ce_1(t) \\ ce_2(t) \end{bmatrix}, \quad (31)$$

with

$$\mathbf{G} = \begin{bmatrix} 0 & 1 \\ 0 & 0 \end{bmatrix} \quad (32)$$

$$H = \begin{bmatrix} 0 \\ 1 \end{bmatrix}, \tag{33}$$

where  $K$  is a feedback gain vector of shape  $[k_1, k_2]$ . Once the feedback gain  $K$  in Equation (31) is set by using a Linear–Quadratic Regulator (LQR) [34], the angular state to be applied on the control masses can be defined. The entire process for the application of a TRD to an SDOF oscillator is illustrated in Figure 3.

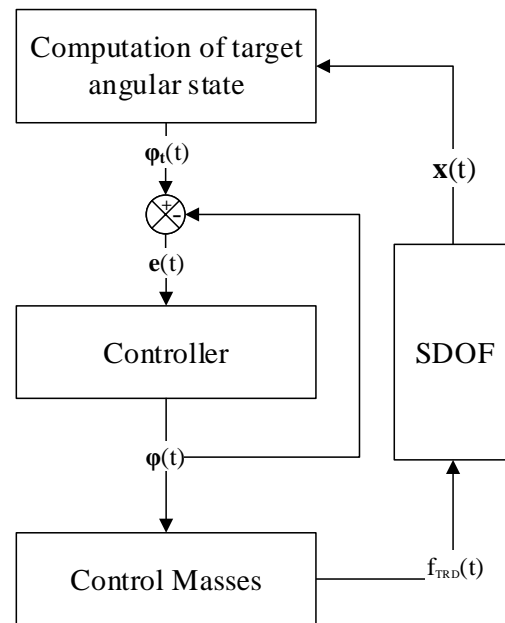


Figure 3. The TRD control for the SDOF oscillator.

### 3. Design of a Damping System with the TRD for Wind Turbine

A wind turbine is a complex structure coupling solid–fluid interactions as well as electromechanics. It is impossible to evaluate the performance of wind turbines under every realistic condition during their lifetime. In the typical design process nowadays, a wind turbine is designed for a set of operating conditions in such a way that, if the environment meets that condition, in reality, the wind turbine should achieve at least the desired performance. A commonly used industrial standard is IEC61400-1 [36], which characterized not only a set of wind conditions but also a variety of incidents and special states.

The TRD will be applied to an aero-hydro-servo-elastic model of wind turbine using FAST. In order to stay as close as possible to the previous context of the SDOF oscillator, we set a Design Load Case (DLC) with a longitudinal wind speed and no other exciting force. A commonly used DLC involving such wind conditions is the Extreme Operating Gust (EOG) [36], in which the wind speed shortly increases to a high level and deflects the whole turbine. This DLC will be combined with a grid-loss event, which consists of quickly stopping the wind turbine operation and adding extra excitations to the wind turbine. Then, the turbine oscillates periodically around its rest position at the wind turbine’s natural frequency.

#### 3.1. NREL 5MW Reference Wind Turbine with FAST Simulation Tools

Many numerical modeling tools have been developed to simulate the dynamics of a wind turbine [37–39]. An open source software, FAST [40], is used in this work. It allows an aero-hydro-servo-elastic coupled simulation considering all the wind turbine components.

FAST simulates the entire wind turbine as a combination of flexible and rigid bodies. Firstly, the wind condition (i.e., a time series of wind speed in the spatial domain) is generated by using its wind speed model based on its definition given in Section 3.2. The dynamic analysis is then carried out by evaluating its aerodynamic model, elastic structure

model, functional model, and the other supplementary models. Finally, the resulting deflections, forces, and moments computed on the tower and blades are exported and can be analyzed.

Two reference wind turbines are commonly used in the field of numerical simulations: (1) NREL offshore 5 MW baseline wind turbine [41]; (2) DTU 10-MW reference wind turbine [42]. Both are initially designed for offshore scenarios. However, an onshore NREL 5 MW reference wind turbine is also part of FAST certification tests, allowing us to validate our model integration into the software. Despite that, there is no real-world implementation or application of the NREL 5 MW turbine, it is still a meaningful reference wind turbine that has been widely studied in academic research and is often used as a benchmark in developing or investigating wind turbine technologies [43–47]. For this reason, this baseline wind turbine is modeled in FAST and served as an initial design for an onshore wind turbine in this work.

The key characteristics of the NREL 5 MW reference wind turbine are mainly based on the specification of the REpower 5M wind turbine and the Dutch Offshore Wind Energy Converter Project (DOWEC) [48]. It is a three-bladed horizontal-axis wind turbine (HAWT) with the key properties given in Appendix A Table A1.

### 3.2. Design Load Case

#### 3.2.1. Wind Condition: Extreme Operating Gust (EOG)

The most essential parameter for characterizing the wind condition is the mean wind speed. It is the mean value of wind speeds measured at hub height over a period of 10 min for several years. The annual mean wind speed at hub height  $V_{avg}$  is imperative for identifying normal conditions as well as extreme conditions.

The wind speed distribution is described by a probability distribution function at hub height. For the normal wind conditions, it is assumed to follow a Rayleigh distribution, that is to say, a Weibull distribution with a shape factor of 2. Equation (34) provides the cumulative probability function for this condition.

$$F(V < V_{hub}) = 1 - \exp \left[ -\pi \left( \frac{V_{hub}}{2V_{avg}} \right)^2 \right] \tag{34}$$

where,  $V_{hub}$  = wind speed at hub height (m/s).

$V_{avg} = 0.2V_{ref}$  based on the wind turbine class specified by designer (m/s)

The wind speed distribution determines the occurrence of individual load condition over wind turbine.

To determine the wind profile (aka vertical wind shear), the Hellmann power-law model is applied with an exponent of 0.2. It describes the mean wind speed as a function of height  $z$  above the ground:

$$V(z) = V_{hub} \left( \frac{z}{z_{hub}} \right)^{0.2}, \tag{35}$$

where,  $z$  = height above ground level (m)

$z_{hub}$  = wind turbine hub height (m).

In order to study the ultimate loads on wind turbines, an extreme wind condition must be designated. The Extreme Operating Gust (EOG) model is involved in the present work. It introduces a Mexican-hat change in wind speed while keeps the same wind direction. This makes it a good choice for investigating the structural responses of the wind turbine tower under ultimate loads.

To be specific, a wind gust is a rapid change in the wind speed. It needs to be characterized by its rise-time, its magnitude and its duration. An EOG is a gust appearing in a short period of time  $T_{gust}$  when the turbine is operating at the same time. By definition, the EOG concerns only the wind velocity in the longitudinal direction (i.e., wind direction).

The horizontal and vertical wind velocities are equal to 0. The magnitude of EOG at hub height  $V_{gust}$  depends on the turbulence standard deviation  $\sigma_1$ , the scale of the turbulence  $\Lambda_1$ , and the rotor diameter of the turbine  $D$ .

$$V_{gust} = \min \left\{ 1.35(V_{e1} - V_{hub}), 3.3 \left( \frac{\sigma_1}{1+0.1\left(\frac{D}{\Lambda_1}\right)} \right) \right\} \tag{36}$$

with  $V_{e1}(z) = 1.12V_{ref} \left( \frac{z}{z_{hub}} \right)^{0.11}$  and  $\sigma_1 = I_{ref}(0.75V_{hub} + 5.6)$ ,

- where,  $V_{e1}$  = annual extreme wind speed (m/s)
- $V_{hub}$  = wind speed at hub height (m/s)
- $\sigma_1$  = standard deviation of wind speed
- $D$  = diameter of the rotor (m)
- $\Lambda_1$  = longitudinal turbulence scale parameter (m).

According to the IEC 61400-1 standard [36], the longitudinal turbulence scale parameter  $\Lambda_1$  at hub height  $z$  is defined as:

$$\Lambda_1 = \begin{cases} 0.7z & \text{if } z \leq 60 \text{ m} \\ 42 & \text{otherwise.} \end{cases} \tag{37}$$

The wind speed of gust is, therefore, given by its magnitude  $V_{gust}$  and its duration  $T_{gust}$ :

$$V(z, t) = \begin{cases} V(z) - 0.37V_{gust} \sin\left(\frac{3\pi t}{T_{gust}}\right) \left(1 - \cos\left(\frac{2\pi t}{T_{gust}}\right)\right) & \text{for } 0 \leq t \leq T_{gust} \\ V(z) & \text{otherwise.} \end{cases} \tag{38}$$

The duration of gust  $T_{gust}$  is set to 10.5 s by the standard [36]. More information about the probability of occurrence, the period and the spatial distribution of the gust can be found in [49].

### 3.2.2. Operating Condition: Grid Loss

In the above section, the magnitude of wind gust  $V_{gust}$  and the wind speed of gust  $V(z, t)$  have been given in Equations (36) and (38), respectively. The duration of gust  $T_{gust}$  is fixed at 10.5 s by IEC 61400-1 specifications [36]. We added a period of 60 s before the wind gust event to avoid the noise in dynamic response. Another 100 s is also added after the wind gust event to track decaying vibration. An illustration of this wind condition is plotted in Figure 4.

The red hatched region in Figure 4 represents the eventual coincidence between the EOG and an electrical fault (i.e., grid loss). The grid loss is an incident that assumes that the connection to the power network is broken due to an internal or external reason. The electrical generator should be shut down immediately by the protection system. Otherwise, the subsequent loading may lead to a resonance between the natural frequency of the tower and that of the rotating blades.

Here, the term “immediately” is numerically selected by the user. In this work, a period of 0.2 s is set to represent the reaction time of the wind turbine protection system. To achieve the worst loading on wind turbine, the timing of grid loss was tested between 0 s and 30.5 s (i.e., the red hatched zone in Figure 4) with a time-step of 0.1 s. The numerical results will be shown and discussed in Section 4.1.

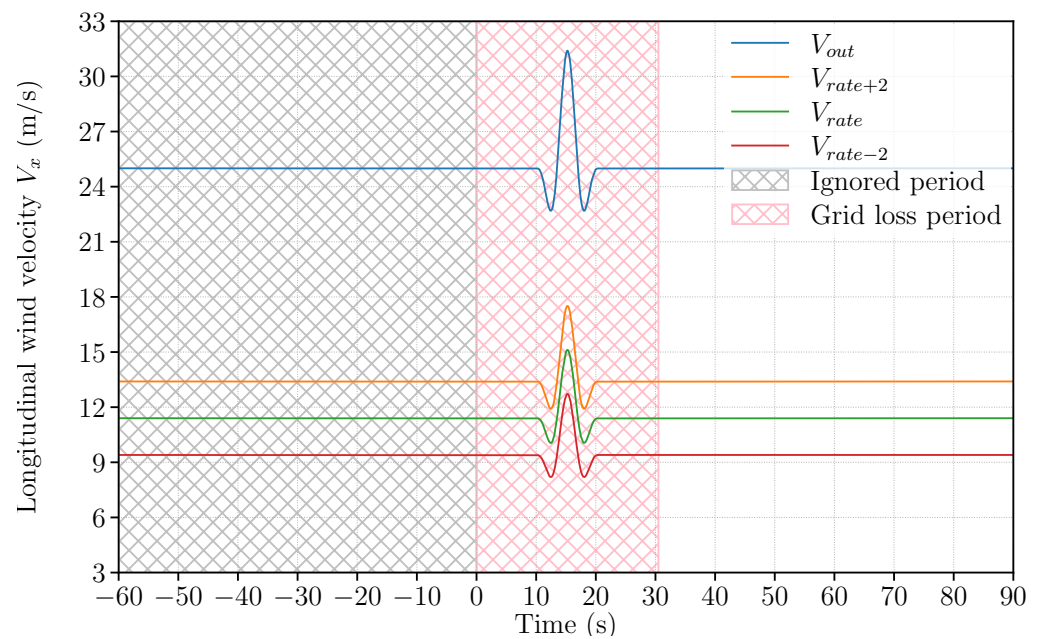


**Figure 4.** Wind velocity at hub height in longitudinal direction with Extreme Operating Gust (EOG).

### 3.3. Numerical Setup of FAST with TRD

A potential engineering design of TRD for a wind turbine is illustrated in Figure 5. Due to the lack of space inside the wind turbine, the TRD is planned to be installed inside the wind turbine tower. The TRD unit could be attached to the inner surface of the tower by six steel beams; more clearly, three beams on the top and three beams on the bottom. This would ensure a rigid connection between the TRD unit and the structure of the wind tower. The actuator would be placed along the centerline of the tower and connected to the beams through an upper bearing and a lower bearing. Then, the two control masses will be hinged to their actuator by rods. Each control mass would likewise be connected to the actuator axis by two rods, that is, an upper one and a lower one.

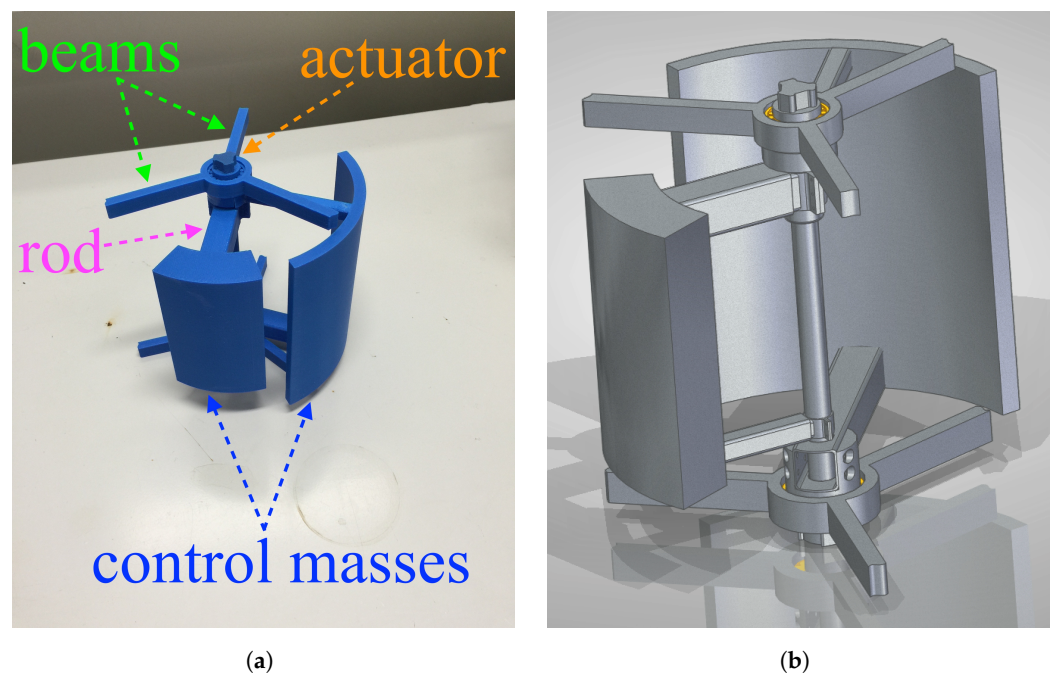


**Figure 5.** Design of the TRD for wind turbine towers: (a) View in maquette. (b) View in CAD (Copyright ©2021 Soletanche Freyssinet. All rights reserved).

When a vibration needs to be damped, the control algorithm of TRD (see Section 2.3.3) will send a signal to the TRD’s actuator to move the rods. Using an electromagnetic coil (or motor-based actuator), the actuator rotates the actuator axis, moving the connecting rods, and consequently rotating the attached control masses. The control masses are made by the same material and have the same mass. However, their layouts and radius (the length of rods) are made to be different so that they can be installed on the different rings (see Figure 5). The product of control mass and radius  $m_c r$  for the rotor on the inner ring is kept the same as that on the outer ring.

The TRD is tuned to reduce the vibration under the most important mode, that is, the natural mode which causes the largest loads on the full-system. Several previous studies [12,50] have identified that the 1st tower fore-aft bending mode is the most important. In this work (see Table A1), it has a natural frequency of 0.324 Hz for this work.

To ensure the function of TRD and prevent the re-excitation of the system, we proposed an event-based ON/OFF control for TRD due to its simplicity and efficiency (Figure 6). It is a closed-loop control based on switching logic and has no intermediate state but only fully ON and fully OFF states. In other words, the control force from TRD  $f_{TRD}(t)$  is instantly applied to the structure without any transition phase between the ON state and the OFF state.

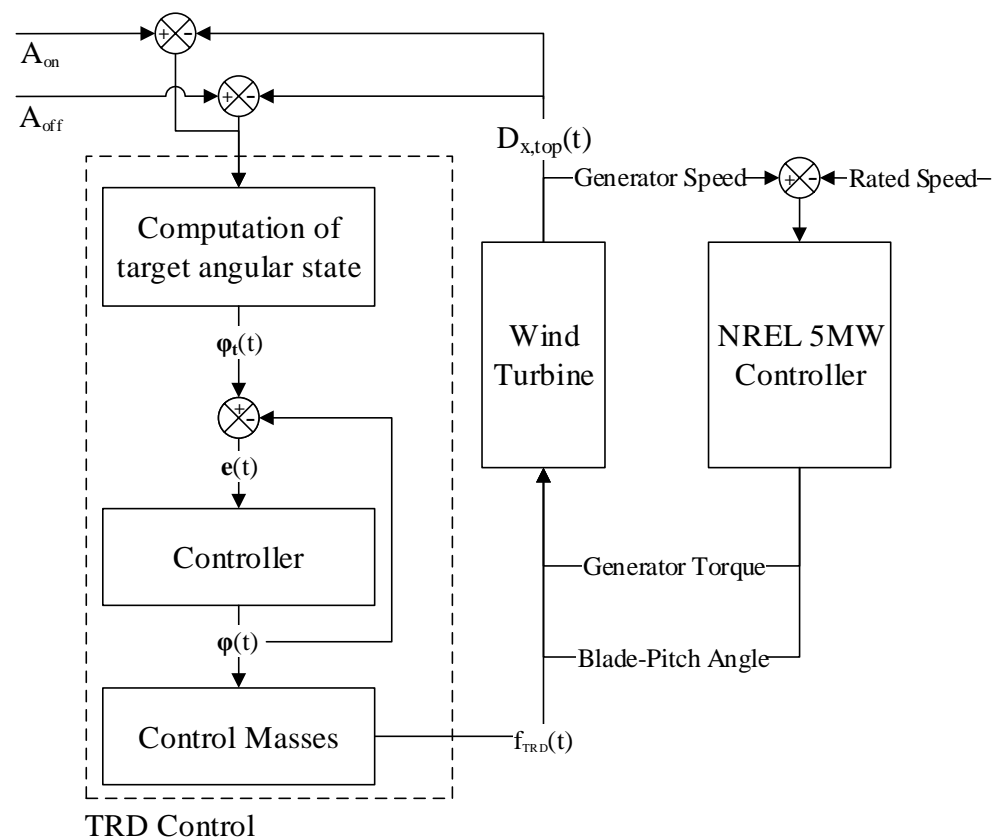


Figure 6. Integration of TRD control to the NREL 5MW reference wind turbine control.

In Figure 6, the default control system of NREL 5MW reference wind turbine [41] is simplified on the right side while the proposed TRD control is represented on the left. The tower-top deflection  $D_{x,top}$  is computed and fed back to the controller of TRD. It is compared to two thresholds of vibration amplitude,  $A_{on}$  and  $A_{off}$ , in the way given in Algorithm 1.

---

**Algorithm 1:** ON/OFF control of the TRD for the wind turbine tower.

---

```

1 if  $D_{x,top} \geq A_{on}$  then
2   | Apply  $f_{TRD}(t)$  on the tower-top
3 end if
4 if  $D_{x,top} \leq A_{off}$  then
5   |  $f_{TRD}(t) = 0$ 
6 end if

```

---

The value of the threshold  $A_{off}$  is set lower than  $A_{on}$ . If the measured deflection  $D_{x,top}$  falls below  $A_{off}$ , the TRD is turned off to avoid the wind turbine being re-excited by the forces generated from the TRD. If  $D_{x,top}$  exceeds  $A_{on}$ , the TRD is turned back on to reduce vibrations of the wind turbine.

Recalling the major properties of NREL 5MW reference wind turbine given in Table A1, the following properties in Table 1 are set to the TRD.

**Table 1.** Properties of TRD for NREL 5MW reference wind turbine.

Property	Value
Total mass of control masses	2.0 t
Radius of TRD	1.0 m
Position of TRD (in tower-base coordinate system)	(0.00, 0.00, 87.60)
Working mode	Mode 1: continuous rotation
Threshold of vibration-amplitude $A_{on}$	0.5 m
Threshold of vibration-amplitude $A_{off}$	0.1 m

Note that the TRD mass is approximately 0.58% of the tower mass and 0.33% of the total mass above ground. From the perspective of mass requirements, this is a feasible design. The TRD is supposed to be positioned on the tower-top (at height of 87.60 m). The inner radius of the tower on the tower-top is 1.910 m, hence, the TRD-to-tower clearance (i.e., available space between the outer radius of TRD and the inner radius of the tower) is 47.64%. This is a feasible TRD size from the perspective of space requirements.

The numerical configurations to model this reference wind turbine in FAST are retrieved from FAST certification tests [40] except for the time-step, which is fixed to 0.1 s based on preliminary sensitivity analysis.

#### 4. Results and Discussion

##### 4.1. EOG with Grid Loss

##### 4.1.1. Evaluation of System Performance without Damper

The performance of the NREL 5MW reference wind turbine under the grid loss condition is firstly evaluated with its default control system. The tower fore-aft deflection  $D_x$  on the tower-top, the fore-aft force  $F_x$  and the pitching moment  $M_y$  on the tower-base are exported as the reference that will be compared to the system performance with TRD in Section 4.2.1. To give an example, the wind tower response at cut-out speed  $V_{out}$  is shown in Figure 7.

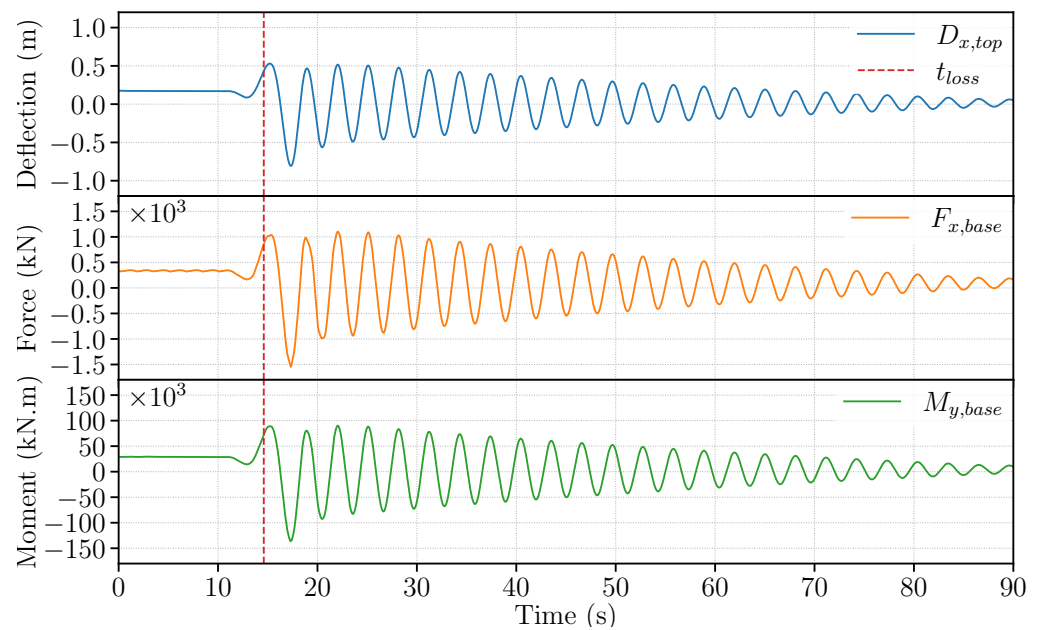


**Figure 7.** Wind turbine tower reactions at cut-out wind speed ( $V_{out} = 25.0$  m/s).

The tower-top fore-aft deflection  $D_x$ , the tower-base fore-aft force  $F_x$  and the tower-base pitching moment  $M_y$  is represented respectively by a blue line, orange line and green line in Figure 7. The red dotted line shows the instant that the grid loss occurs in the electrical network. A large change in the peak-to-peak amplitude is observed in all types of the tower reaction after the electrical fault. Since the structural damping ratio of the wind turbine tower is small (see Table A1), the energy dissipation is really weak that leads the tower to still oscillate at the end of the simulation ( $t = 90$  s). This exposes the need for a damping system that is expected to stabilize the wind tower after the grid loss and keep the structure safely. Before that, it is necessary to figure out the most unfavorable load case resulting in the maximum loading on the system.

#### 4.1.2. Grid Loss Timing

To quantify the worst loading on wind turbine, the fore-aft tower deflection  $D_x$  on tower-top and the fore-aft force  $F_x$  and the pitching moment  $M_y$  on tower-base is considered. For each response simulation, the maximum magnitude of  $D_x(t)_{max}$ ,  $F_x(t)_{max}$  and  $M_y(t)_{max}$  are exported. The timing of grid loss  $t_{loss}$  is chosen when the magnitude of response reaches its maximal value across all simulations, that is,

$$t_{loss} = \tau \text{ s.t. } U(t)_{max}^{grid \text{ loss} = t_{loss}} = \max \left\{ U(t)_{max}^{grid \text{ loss} = \tau} \right\} \text{ where } \tau \in [10.0, 10.1, \dots, 30.5], \quad (39)$$

where  $U$  stands for a type of mechanical response such as deflection  $D_x$ , force  $F_x$  or moment  $M_y$ . The results for the considered mean wind speed of EOG are listed in Table 2.

**Table 2.** Grid loss timing to achieve the worst loading on wind turbine.

Mean Wind Speed ( $V_{mean}$ )	Grid Loss Time $t_{loss}$ (s)		
	$\max\{D_{x,top}\}$	$\max\{F_{x,base}\}$	$\max\{M_{y,base}\}$
$V_{out}$ (25.0 m/s)	14.9	14.9	14.9
$V_{rate+2}$ (13.4 m/s)	14.8	14.8	14.8
$V_{rate}$ (11.4 m/s)	14.6	14.6	14.6
$V_{rate-2}$ (9.4 m/s)	14.7	14.7	14.7

From Equation (38), the wind speed reaches its maximum at 15.25 s. Table 2 shows that the tower response reaches its maximum when the grid loss occurs just before the peak of longitudinal wind velocity, in other words, the loading on turbine reaches its highest values.

To better understand the grid loss timing and the consequent loading, the considered mean wind speed  $V_{mean}$  is extended to the range of [3, 25] at a step of 0.1 m/s. Figure 8 illustrates the relation between the grid loss, the mean wind speed and the subsequent loading. To clearly discuss the grid loss timing, an example of wind gust at  $V_{out}$  is given in the upper line-chart while a contour-chart is plotted in the lower part to demonstrate the peak-to-peak amplitude of fore-aft deflection  $D_{x,top}$ . The ordinate axis of the upper chart is a longitudinal component of the instantaneous wind speed  $V_x$ , whereas the ordinate axis of the lower chart is the mean wind speed  $V_{mean}$ . Both the abscissae axes correspond to the duration of a wind gust. In the lower chart, the isolines represent the peak-to-peak amplitude of deflection  $D_{x,top}$  subjected to the grid loss at different times and different mean wind speeds. The color bar next to the lower chart clarifies the level-set for these peak-to-peak amplitudes.

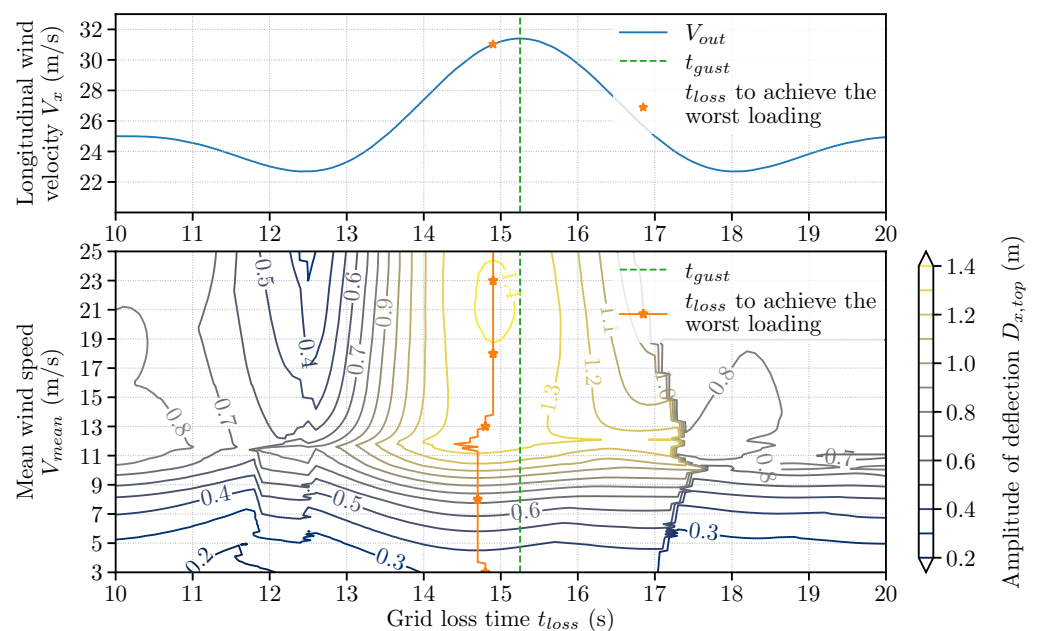


**Figure 8.** Grid loss timing in the range of operating wind speed with reference to tower deflection. The upper line plot gives an example of wind speed of gust at mean wind speed  $V_{mean} = V_{out} = 25$  m/s. The lower contour plot shows the peak-to-peak amplitude in relation to the mean wind speed  $V_{mean}$  and the grid loss time  $t_{loss}$ .

For  $V_{mean}$  between  $V_{rate-2}$  (9.4 m/s) and  $V_{rate+2}$  (13.4 m/s), the peak-to-peak amplitude of  $D_{x,top}$  increases progressively and depends mainly on the grid loss instant  $t_{loss}$ . When  $t_{loss}$  approaches the time of maximum wind gust speed  $t_{gust}$  (green dashed line in Figure 8), the amplitude becomes higher and higher. Lastly, for  $V_{mean}$  greater than  $V_{rate+2}$  (13.4 m/s), the peak-to-peak amplitude of fore-aft deflection has a similar fluctuation to that of wind velocity, that is, a trough area of amplitude in 12 s to 13 s and 17.5 s to 18.5 s along with a peak area in 14.5 s to 15.5 s.

For mean wind speed below  $V_{rate-2}$  (9.4 m/s), the effect of grid loss before or after the maximum wind gust speed, which occurs at  $t_{gust} = 15.25$  s, is not significant. The subsequent deflection  $D_{x,top}$  has a peak-to-peak amplitude less than 0.7 m.

#### 4.1.3. Discussions

The timing of grid loss to achieve the worst loading (i.e., the orange line in Figure 8) lies always before the occurrence of maximum wind speed. It is within the range of

$[t_{loss} - 1, t_{loss}]$  in general. When mean wind speed  $V_{mean}$  goes higher, the peak-to-peak amplitude gets higher.

The above research extends the EOG from four wind speeds specified in the IEC61400-1 standard to the full range of operating wind speeds. It indicates the timing for grid loss to achieve the worst loading at any mean wind speed in the EOG condition. The same conclusion can be stated with regard to the local tower force and the local tower moment on tower-base (see Figures A1 and A2 in Appendix A). In the next section, the grid loss is set to the timing at which the peak-to-peak amplitude reaches the maximum for all mean wind speeds between  $V_{in}$  and  $V_{out}$ .

#### 4.2. Evaluation of TRD Performance

A passive TMD has been designed for the same reference wind turbine so that we could compare the performance of the TRD to a reference damper which is designed under the same requirements. The mass of the TMD is set to the same as the mass of the TRD. The TMD is also supposed to be installed on the tower-top. The other TMD parameters are set to minimize the displacement according to Den Hartog’s design [51]. The TMD is simulated under the same load conditions (i.e., EOG with grid loss). All the TMD parameters can be found in Table 3.

**Table 3.** Properties of TMD for NREL 5MW reference wind turbine.

Property	Value
Mass	2 t
Position of TMD (in tower-base coordinate system)	(0.00, 0.00, 87.60)
Damped natural angular frequency $\omega_{n,d}$	2.030 rad/s
Stiffness	8245 N/m
Viscous damping	252 N/(m/s)

Note that the TMD described above is to evaluate the effectiveness of the TRD under the same design limits. Many researchers [12,17] suggest that the optimal mass ratio of a TMD for wind turbines is between 2% and 5%.

##### 4.2.1. Results

The above analysis shows that the intense vibrations with high amplitude have occurred on the tower-top under the combination of gusty wind and the loss of the power network. After investigating the mean wind speed  $V_{mean}$  and the grid loss timing  $t_{loss}$ , we find out that the amplitude of the fore-aft deflection on tower-top is maximized when the mean wind speed  $V_{mean}$  approaches the cut-out speed  $V_{out}$  (see Figure 8). Thereupon, both the TMD and the TRD are simulated in the EOG wind condition at the mean wind speed of  $V_{out}$ . As an active damper, the TRD parameters (Section 3.3) and the TRD control algorithm (Section 2.3.3) are integrated to FAST. As a passive damper, only the TMD parameters developed in Section 4.2 are considered in numerical simulations. Equation (40) is used to evaluate the effectiveness of the damper by comparing it to the tower response obtained without any damper plotted in Figure 7.

The fore-aft deflection on the tower-top  $D_{x,top}$  without the damper is used as the reference response and is plotted by the blue dotted line in Figure 9. Meanwhile, the tower response with the TMD is presented by the orange dashed line, and that with the TRD is shown in green. The grid loss time  $t_{loss}$  is marked by the red dashed line. It is clear that the tower-top fore-aft deflection  $D_{x,top}$  simulated with a passive or active damper has an amplitude smaller than that without any damper.

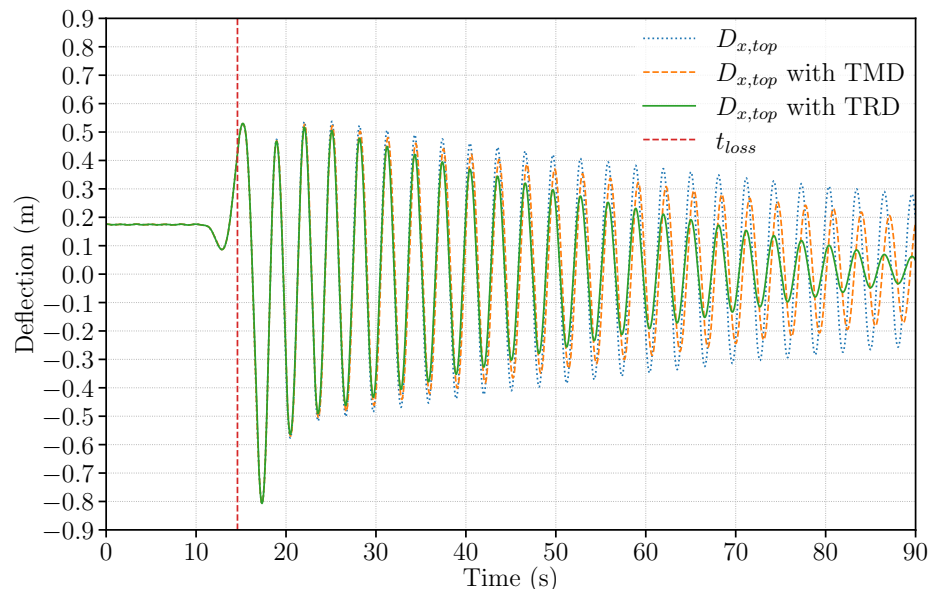


Figure 9. Tower-top fore-aft deflection at cut-out wind speed ( $V_{out} = 25.0$  m/s) with/without damper.

At the end of simulation ( $t = 90$  s), the reference fore-aft deflection (blue dotted line) still oscillates between  $-0.26$  m and  $0.28$  m. In the case of passive damper TMD (orange dashed line), the vibration is limited between  $-0.17$  m and  $0.21$  m. The peak-to-peak amplitude is reduced by 30% according to Equation (40). In the case of the active damper TRD (green line), the vibration is stabilized between  $-0.03$  m and  $0.06$  m. That is a reduction of 83% in terms of peak-to-peak amplitude.

Figure 10 reveals the status of TRD during the simulated time through three charts. The first chart on the top is similar to Figure 9 showing the fore-aft deflection on the tower-top; the second one in the middle draws the forces generated by the TRD while the last chart on the bottom shows the signal sent from the controller of the TRD. Once the amplitude of the fore-aft deflection  $A_{x,top}$  passed the threshold  $A_{on} = 0.5$ , the TRD is activated. It retains active until the amplitude  $A_{x,top}$  is smaller than  $A_{off} = 0.1$  (see the cyan line in the bottom chart). As expected, the force created by the TRD (yellow line in the middle chart) retains a sinusoidal signal with a phase shift of  $\frac{T_{def}}{2}$ , where  $T_{def}$  is the period of the fore-aft deflection on the tower-top presented by the orange line in the top chart.

#### 4.2.2. Discussions

As shown in Figure 9, the amplitude of vibration is significantly reduced by the TRD compared to that with the TMD under the same load condition. At the moment when TRD is turned off (around  $t = 87$  s), the peak-to-peak amplitude of fore-aft deflection with TRD reaches  $0.09$  m as expected, but, for the TMD, the peak-to-peak amplitude still remains at  $0.39$  m. In order to evaluate the effectiveness of the TRD, the reduction rate on the peak-to-peak amplitude is used. It is computed by:

$$\epsilon = \left| \frac{A_{\text{with damper}} - A_{\text{without damper}}}{A_{\text{without damper}}} \right| \times 100\%. \tag{40}$$

Table 4 summarizes the performance of the TRD and the TMD under all mean wind speed required by the standard IEC61400-1. All results are taken at the moment of deactivating the TRD, see the purple dashed line in Figure 10. Despite the operating mean wind speed, the TMD reduces the peak-to-peak amplitude of the tower response by 9% to 29%. For the TRD, the amplitude is reduced by 60% to 83%. The TRD outperforms the TMD by at least three and up to six times in terms of amplitude reduction. The higher the mean wind speed is, the more effective the TRD is.

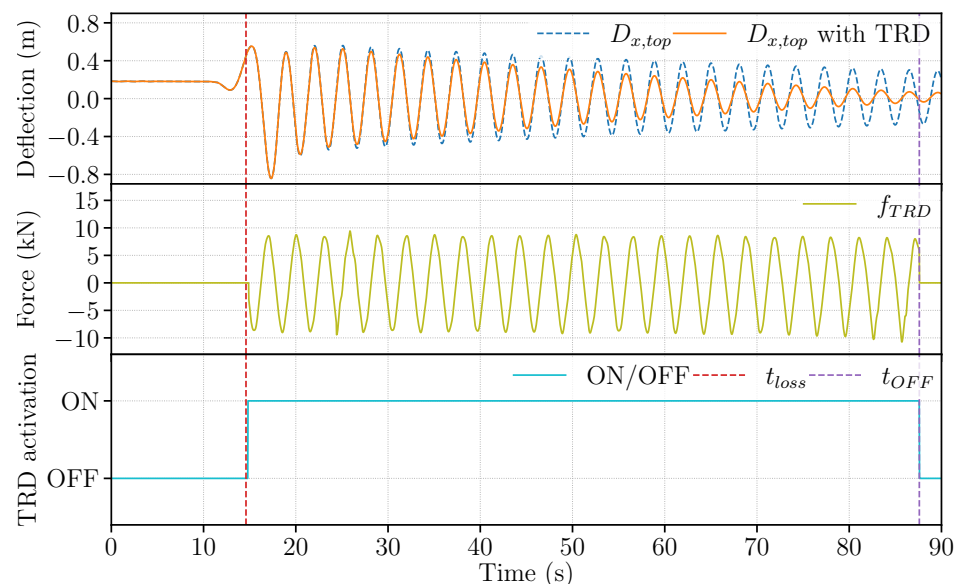


Figure 10. Status of TRD in DLC2.3 at  $V_{out}$  (the time dependency is omitted in the legend).

Table 4. Peak-to-peak amplitude of the tower response (with the reduction rate  $\epsilon$  presented between parenthesis).

		$V_{out}$	$V_{rate+2}$	$V_{rate}$	$V_{rate-2}$
$D_{x,top}$ Deflection (m)	without damper	0.54	0.44	0.33	0.20
	with TMD	0.39 (−27.78%)	0.35 (−20.45%)	0.27 (−18.18%)	0.18 (−10.0%)
	with TRD	0.09 (−83.33%)	0.08 (−81.82%)	0.08 (−75.76%)	0.08 (−60.00%)
$F_{x,base}$ Force (kN)	without damper	1084	898	656	408
	with TMD	761 (−29.80%)	696 (−22.49%)	548 (−16.46%)	367 (−10.05%)
	with TRD	195 (−82.01%)	179 (−80.07%)	161 (−75.46%)	159 (−61.03%)
$M_{y,base}$ Moment (kN.m)	without damper	$92.1 \times 10^3$	$76.0 \times 10^3$	$56.1 \times 10^3$	$34.8 \times 10^3$
	with TMD	$64.8 \times 10^3$ (−29.64%)	$59.4 \times 10^3$ (−21.84%)	$46.4 \times 10^3$ (−17.29%)	$31.6 \times 10^3$ (−9.20%)
	with TRD	$16.1 \times 10^3$ (−82.52%)	$15.2 \times 10^3$ (−80.00%)	$13.7 \times 10^3$ (−75.58%)	$13.7 \times 10^3$ (−60.63%)

All these numerical results prove that the TRD is notably effective in reducing vibrations of the wind tower under the gusty wind. More results can be found in the appendix where the performance of TRD is evaluated at a mean wind speed of  $V_{rate+2}$  (Figure A3),  $V_{rate}$  (Figure A4) and  $V_{rate-2}$  (Figure A5).

### 5. Conclusions

In this paper, we introduced a new active damping system for wind turbines to reduce the vibrations of a wind turbine tower. The twin rotor damper (TRD) is primarily used as a damping system for a single degree of freedom (SDOF) oscillator. The simulation tool FAST has been modified to take this newly designed damping system into consideration as well as the coupled dynamics during aero-elastic wind turbine simulations. To evaluate the performance of the proposed system, an idealistic load case in which the TRD model could be efficient has been designed. The extreme operating gust (EOG) model from the IEC61400-1 standard is applied to involve a rapid change of wind velocity in a unidirectional wind flow. The loss of the power network leads to a significant change in the magnitude of the structural dynamic response. The coincidence between these two events is studied. It reveals the timing for involving the maximum loading on the structure for all mean wind speeds in the operating range. Under those conditions, the wind turbine is first bent by the wind gust, then released by the grid loss, and finally vibrates at its natural mode. The efficiency of the TRD is shown to be three to six times more efficient than a passive tuned mass damper (TMD) of a similar weight. Further development of the proposed system will be conducted to allow multi-directional damping, which could be done by adding a

phase angle between the two control masses. The observer part of our controller could also be improved in order to couple the target angular position of the TRD to any measured velocity on top of the tower. This could be investigated with the alternative swinging mode of operation or by applying the method proposed in [52] for targeting non-harmonic vibrations. The efficiency of the TRD should also be evaluated considering the realistic behavior of the actuator, which needs time to reach the desired position or velocity. Last but not least, the gain in the power production and the reliability of wind turbines from this promising system should be evaluated as well.

**Author Contributions:** Conceptualization, methodology and data curation, H.B.; formal analysis and validation, Y.A.; software, J.-M.C.; supervision, D.L.; writing—original draft preparation, H.B.; writing—review and editing, Y.A. All authors have read and agreed to the published version of the manuscript.

**Funding:** This research was funded by the French Ministry of Higher Education, Research and Innovation through a grant from INSA Rouen Normandie for a Ph.D. thesis.

**Acknowledgments:** All authors would like to acknowledge the administrative support from Prof. Edgar Emilio Bastidas-Arteaga and the technical support from Prof. Dr.-Ing. Uwe Starossek. We also appreciate the support from Freyssinet Sustainable Technology.

**Conflicts of Interest:** The authors declare no conflict of interest.

### Abbreviations

The following abbreviations are used in this manuscript:

DLC	Design Load Case
EOG	Extreme Operating Gust
HAWT	Horizontal-Axis Wind Turbine
NREL	National Renewable Energy Laboratory
FAST	Fatigue, Aerodynamic, Structure and Turbulence codes
TRD	Twin Rotor Damper
TMD	Tuned Mass Damper
SDOF	Single Degree Of Freedom
PAC	Pitch Angle Control

## Appendix A

### Appendix A.1

**Table A1.** Overview of NREL 5MW baseline wind turbine.

Component	Property	Value
Blade	Variable-speed collective pitch control	-
	Number of blades	3
	Mass	17.74 t
Rotor	Rotor mass	110 t
	Cut-in wind speed	3.0 m/s
	Rated wind speed	11.4 m/s
	Cut-out wind speed	25.0 m/s
Hub and nacelle	Hub mass	56.78 t
	Hub height	90.00 m
	Elevation of yaw bearing above ground	87.60 m
	Nacelle mass	240 t
Drivetrain	High-speed multiple-stage gearbox	-
	High-speed shaft brake time	0.6 s
Tower	Mass	347.46 t
	Density	8500 kg/m <sup>3</sup>
	Young's modulus	210 GPa
	Shear modulus	80.8 GPa
	Poisson's ratio	0.3
	1st full-system natural frequency (tower fore-aft)	0.324 Hz
	Structural damping ratio under all modes	1.00%

Appendix A.2

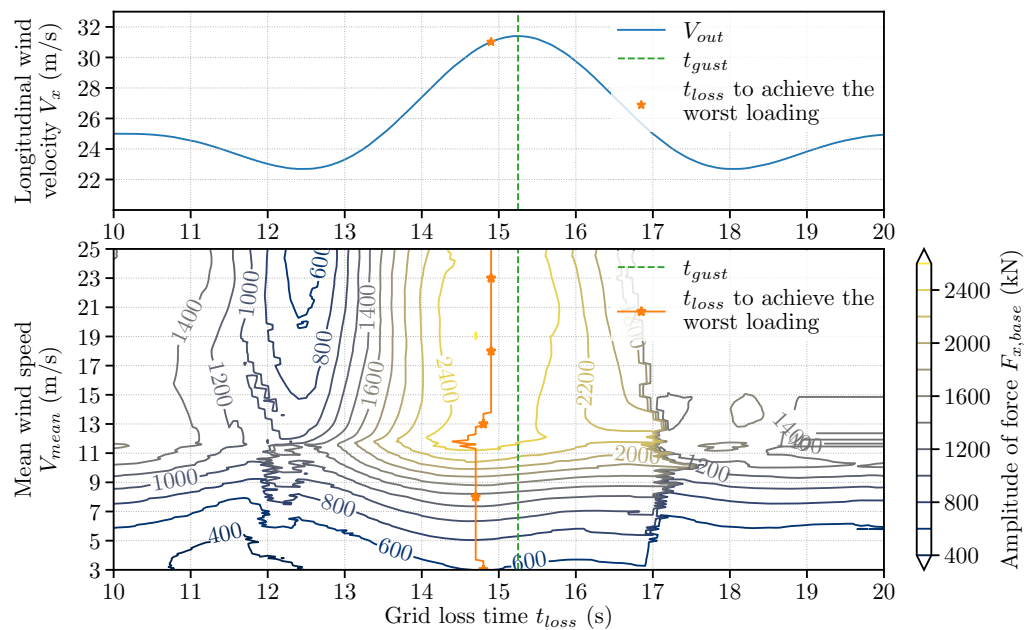


**Figure A1.** Grid loss timing in the range of operating wind speed with reference to tower force. The upper line plot gives an example of wind speed of gust at mean wind speed  $V_{mean} = V_{out} = 25$  m/s. The lower contour plot shows the peak-to-peak amplitude in relation to the mean wind speed  $V_{mean}$  and the grid loss time  $t_{loss}$ .

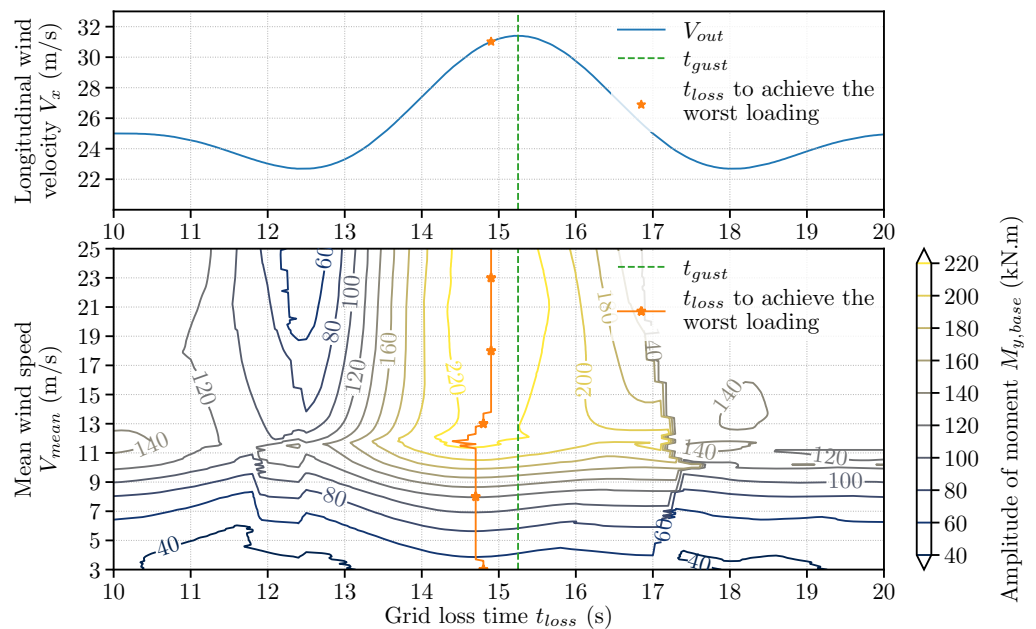


**Figure A2.** Grid loss timing in the range of operating wind speed with reference to tower moment. The upper line plot gives an example of wind speed of gust at mean wind speed  $V_{mean} = V_{out} = 25$  m/s. The lower contour plot shows the peak-to-peak amplitude in relation to the mean wind speed  $V_{mean}$  and the grid loss time  $t_{loss}$ .

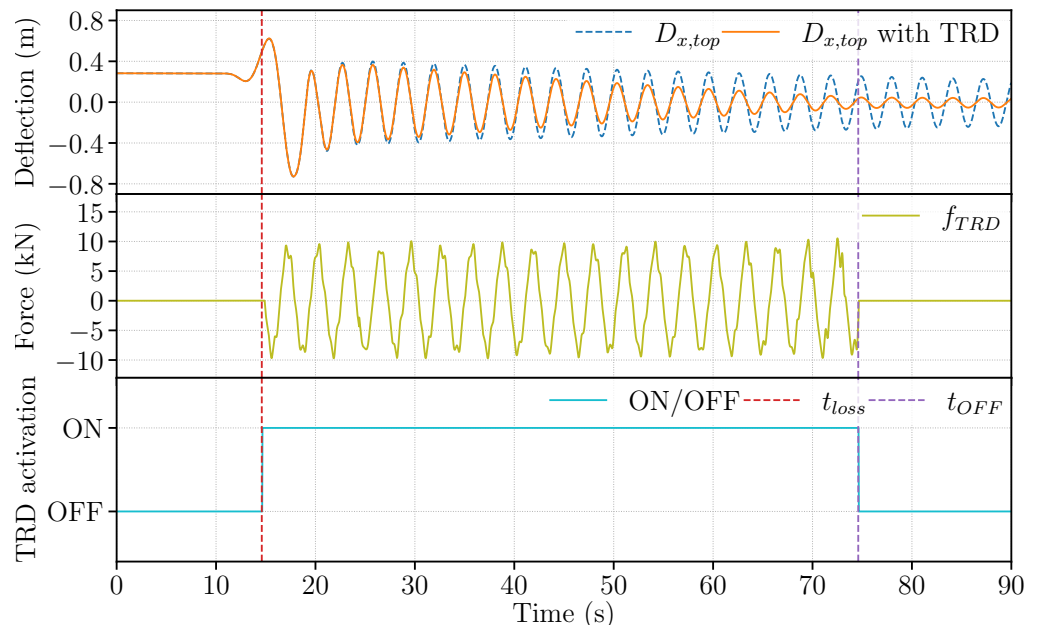


**Figure A3.** Tower-top fore-aft deflection and status of TRD in EOG with grid loss at  $V_{rate+2}$  (the time dependency is omitted in legend).

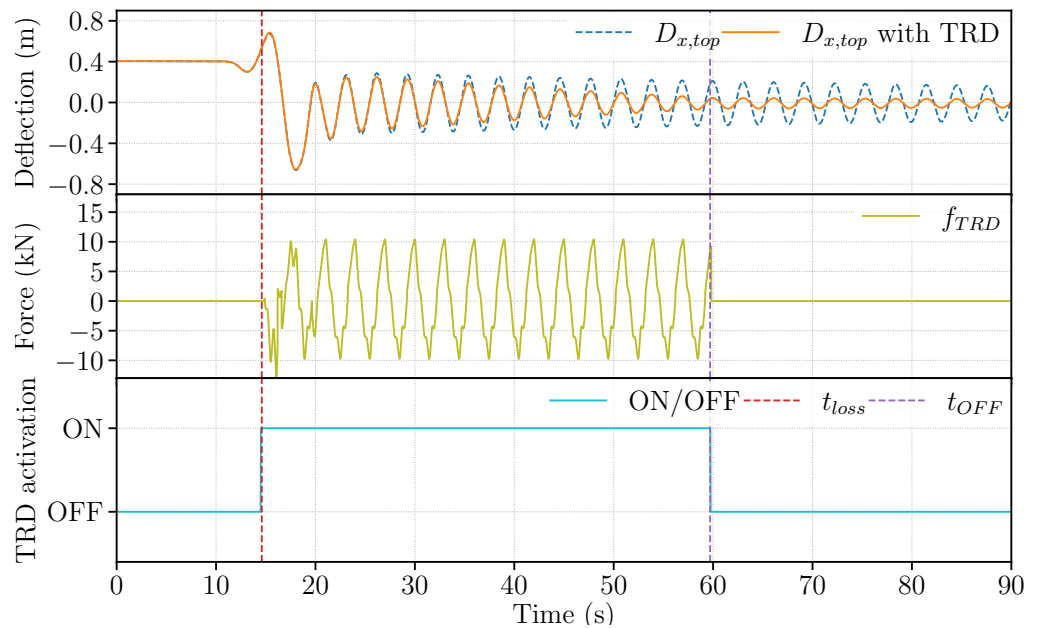


**Figure A4.** Tower-top fore-aft deflection and status of TRD in EOG with grid loss at  $V_{rate}$  (the time dependency is omitted in legend).

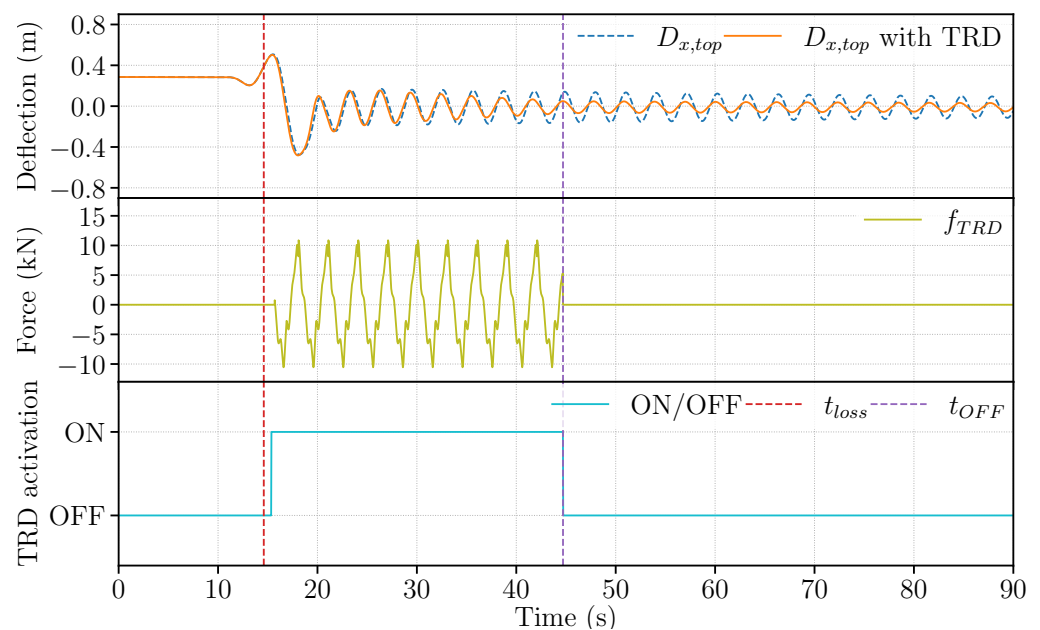


**Figure A5.** Tower-top fore-aft deflection and status of TRD in EOG with grid loss at  $V_{rate-2}$  (the time dependency is omitted in legend).

## References

1. Mohammadi, E.; Fadaeinedjad, R.; Moschopoulos, G. Implementation of internal model based control and individual pitch control to reduce fatigue loads and tower vibrations in wind turbines. *J. Sound Vib.* **2018**, *421*, 132–152. [\[CrossRef\]](#)
2. Lio, W.H.; Jones, B.L.; Rossiter, J.A. Estimation and Control of Wind Turbine Tower Vibrations Based on Individual Blade-Pitch Strategies. *IEEE Trans. Control Syst. Technol.* **2019**, *27*, 1820–1828. [\[CrossRef\]](#)
3. Fitzgerald, B.; Staino, A.; Basu, B. Wavelet-based individual blade pitch control for vibration control of wind turbine blades. *Struct. Control Health Monit.* **2019**, *26*, e2284. [\[CrossRef\]](#)
4. Weber, F.; Feltrin, G.; Huth, O. *Guidelines for Structural Control*; Technical Report March, Swiss Federal Laboratories for Materials Science and Technology (EMPA); Structural Engineering Research Laboratory: Dübendorf, Switzerland, 2006.
5. Weber, F. Semi-active vibration absorber based on real-time controlled MR damper. *Mech. Syst. Signal Process.* **2014**, *46*, 272–288. [\[CrossRef\]](#)
6. Shi, L.; Wang, Y.; Liao, M.; Jiang, Y. *Approach and Application of Semi-Blind Source Separation for Aero-Engine Vibration Signals Using ICA-R*; Journal of Physics: Conference Series; IOP Publishing: Bristol, UK, 2019; Volume 1215, p. 12030. [\[CrossRef\]](#)
7. Kaveh, A.; Javadi, S.M.; Mahdipour Moghanni, R. Optimal structural control of tall buildings using tuned mass dampers via chaotic optimization algorithm. *Structures* **2020**, *28*, 2704–2713. [\[CrossRef\]](#)
8. Jiménez-Alonso, J.F.; Soria, J.M.; Díaz, I.M.; Guillen-González, F. A common framework for the robust design of tuned mass damper techniques to mitigate pedestrian-induced vibrations in lively footbridges. *Structures* **2021**, *34*, 1276–1290. [\[CrossRef\]](#)
9. Jin, C.; Chung, W.C.; Kwon, D.S.; Kim, M.H. Optimization of tuned mass damper for seismic control of submerged floating tunnel. *Eng. Struct.* **2021**, *241*, 112460. [\[CrossRef\]](#)
10. Si, Y.; Karimi, H.R.; Gao, H. Modelling and optimization of a passive structural control design for a spar-type floating wind turbine. *Eng. Struct.* **2014**, *69*, 168–182. [\[CrossRef\]](#)
11. Tong, X.; Zhao, X.; Karcianas, A. Passive vibration control of an offshore floating hydrostatic wind turbine model. *Wind Energy* **2018**, *21*, 697–714. [\[CrossRef\]](#)
12. Stewart, G.; Lackner, M. Offshore wind turbine load reduction employing optimal passive tuned mass damping systems. *IEEE Trans. Control Syst. Technol.* **2013**, *21*, 1090–1104. [\[CrossRef\]](#)
13. Li, C.; Zhuang, T.; Zhou, S.; Xiao, Y.; Hu, G. Passive vibration control of a semi-submersible floating offshore wind turbine. *Appl. Sci.* **2017**, *7*, 509. [\[CrossRef\]](#)
14. Murtagh, P.J.; Ghosh, A.; Basu, B.; Broderick, B.M. Passive control of wind turbine vibrations including blade/tower interaction and rotationally sampled turbulence. *Wind Energy* **2008**, *11*, 305–317. [\[CrossRef\]](#)
15. Yu, W.; Lemmer, F.; Cheng, P.W. Performance of a passive tuned liquid column damper for floating wind turbines. In Proceedings of the International Conference on Offshore Mechanics and Arctic Engineering-OMAE, American Society of Mechanical Engineers Digital Collection, Glasgow, UK, 9–14 June 2019; Volume 10. [\[CrossRef\]](#)

16. Prasad, B.B.; DuVigneau, F.; Woschke, E.; Juhre, D. Wind turbine blade and generator test specimen for evaluating a passive vibration reduction concept based on granular materials. In Proceedings of the ISMA 2020-International Conference on Noise and Vibration Engineering and USD 2020-International Conference on Uncertainty in Structural Dynamics, Leuven, Belgium, 7–9 September 2020; pp. 3525–3539.
17. Fitzgerald, B.; Basu, B. Cable connected active tuned mass dampers for control of in-plane vibrations of wind turbine blades. *J. Sound Vib.* **2014**, *333*, 5980–6004. [[CrossRef](#)]
18. Coudurier, C.; Lepreux, O.; Petit, N. Passive and semi-active control of an offshore floating wind turbine using a tuned liquid column damper. *IFAC-PapersOnLine* **2015**, *28*, 241–247. [[CrossRef](#)]
19. Yao, X.; Liu, Y.; Xing, Z.; Zhang, C. Active vibration control strategy based on expert PID pitch control of variable speed wind turbine. In Proceedings of the 11th International Conference on Electrical Machines and Systems, ICEMS 2008, Wuhan, China, 17–20 October 2008; pp. 635–639.
20. Gambier, A.; Nazaruddin, Y.Y. *Collective Pitch Control with Active Tower Damping of a Wind Turbine by Using a Nonlinear PID Approach*; IFAC-PapersOnLine; Elsevier: Amsterdam, The Netherlands, 2018; Volume 51, pp. 238–243. [[CrossRef](#)]
21. Lara, M.; Garrido, J.; Vázquez, F. Adaptive pi control and active tower damping compensation of a wind turbine. *Renew. Energy Power Qual. J.* **2020**, *18*, 339–344. [[CrossRef](#)]
22. Bai, H. Machine Learning Assisted Probabilistic Prediction of Long-Term Fatigue Damage and Vibration Reduction of Wind Turbine Tower Using Active Damping System. Ph.D. Thesis, INSA Rouen Normandie, Rouen, France, 2021.
23. Gambier, A. Simultaneous design of pitch control and active tower damping of a wind turbine by using multi-objective optimization. In Proceedings of the 1st Annual IEEE Conference on Control Technology and Applications, CCTA 2017, Hawaii, HI, USA, 26–29 August 2017; Volume 2017, pp. 1679–1684. [[CrossRef](#)]
24. Preumont, A.; Seto, K. *Active Control of Structures*; Wiley Online Library: Hoboken, NJ, USA, 2008; pp. 1–296. [[CrossRef](#)]
25. Scheller, J. Power-Efficient Active Structural Vibration Control by Twin Rotor dampers. Ph.D. Thesis, Hamburg University of Technology, Hamburg, Germany, 2014.
26. Korkmaz, S. A review of active structural control: Challenges for engineering informatics. *Comput. Struct.* **2011**, *89*, 2113–2132. [[CrossRef](#)]
27. Rodríguez Tsouroukdissian, A.; Carcangiu, C.E.; Pineda, I.; Fischer, T.; Kuhnle, B.; Scheu, M.; Martin, M. *Wind Turbine Structural Damping Control for Tower Load Reduction*; Conference Proceedings of the Society for Experimental Mechanics Series; Springer: Berlin, Germany, 2011; Volume 4, pp. 141–153. [[CrossRef](#)]
28. Starossek, U. Device for Vibration Control of a Structure. Patent No. US9169894B2, 20 May 2015.
29. Bäumer, R.; Starossek, U. Active vibration control using centrifugal forces created by eccentrically rotating masses. *J. Vib. Acoust.* **2016**, *138*, 041018. [[CrossRef](#)]
30. Bäumer, R.; Terrill, R.; Wollnack, S.; Werner, H.; Starossek, U. Twin rotor damper for the damping of stochastically forced vibrations using a power-efficient control algorithm. *J. Sound Vib.* **2018**, *413*, 308–331. [[CrossRef](#)]
31. Durbin, J.; Koopman, S.J. *Time Series Analysis by State Space Methods*; Oxford University Press: Oxford, UK, 2012.
32. Ogata, K. *Modern Control Engineering*, 5th ed.; Prentice Hall: Upper Saddle River, NJ, USA, 2010.
33. Franklin, G.F.; Powell, J.D.; Emami-Naeini, A. *Feedback Control of Dynamic Systems*, 8th ed.; Pearson: London, UK, 2019.
34. Bäumer, R. Active Vibration Control Using the Centrifugal Forces of Eccentrically Rotating Masses. Ph.D. Thesis, Hamburg University of Technology, Hamburg, Germany, 2017.
35. Bäumer, R.; Starossek, U.; Scheller, J. Continuous state feedback control for twin rotor damper. In Proceedings of the International Conference on Structural Dynamic, EURO-DYN, Porto, Portugal, 30 June–2 July 2014; Volume 2014, pp. 1647–1654.
36. International Electrotechnical Commission (IEC). *Wind Turbines-Part1: Design Requirements*; IHS Markit: London, UK, 2005.
37. Jimack, P.K.; Topping, B.H.V. An overview of parallel dynamic loadbalancing for parallel adaptive computational mechanics codes. In *Parallel and Distributed Processing for Computational Mechanics: Systems and Tools*; Saxe-Coburg Publications: Kippen, UK, 1999; pp. 350–369.
38. Larsen, T.J.; Hansen, A.M. *How 2 HAWC2, the User's Manual*; DTU Wind Energy: Roskilde, Denmark, 2007.
39. Bottasso, C.L.; Croce, A. *Cp-Lambda a Code for Performance, Loads, Aeroelasticity by Multi-Body Dynamics Analysis*; Technical Report; Technical University of Munich (TUM): München, Germany, 2016.
40. Jonkman, J.M.; Buhl, M.L., Jr. *FAST User's Guide*; National Renewable Energy Laboratory (NREL): Golden, CO, USA, 2005; p. 143.
41. Jonkman, J.M.; Butterfield, S.; Musial, W.; Scott, G. *Definition of a 5-MW Reference Wind Turbine for Offshore System Development*; Technical Report February; National Renewable Energy Laboratory (NREL): Golden, CO, USA, 2009. [[CrossRef](#)]
42. Bak, C.; Zahle, F.; Bitsche, R.; Yde, A.; Henriksen, L.C.; Natarajan, A.; Hansen, M.H. *Description of the DTU 10 MW Reference Wind Turbine*; Technical Report July; Technical University of Denmark: Lyngby, Denmark, 2013. [[CrossRef](#)]
43. Di Paolo, M.; Nuzzo, I.; Caterino, N.; Georgakis, C.T. A friction-based passive control technique to mitigate wind induced structural demand to wind turbines. *Eng. Struct.* **2021**, *232*, 111744. [[CrossRef](#)]
44. Arcigni, F.; Abhinav, K.A.; Collu, M.; Venturini, M. Analysis of tripod supported offshore wind turbines under conditions of marine growth. *Ocean Eng.* **2021**, *220*, 108441. [[CrossRef](#)]
45. Lee, H.M.; Kwon, O.J. Performance improvement of horizontal axis wind turbines by aerodynamic shape optimization including aeroelastic deformation. *Renew. Energy* **2020**, *147*, 2128–2140. [[CrossRef](#)]

46. Cheng, P.; Huang, Y.; Wan, D. A numerical model for fully coupled aero-hydrodynamic analysis of floating offshore wind turbine. *Ocean Eng.* **2019**, *173*, 183–196. [[CrossRef](#)]
47. Ebrahimi, A.; Movahhedi, M. Power improvement of NREL 5-MW wind turbine using multi-DBD plasma actuators. *Energy D* **2017**, *146*, 96–106. [[CrossRef](#)]
48. Kooijman, H.; Lindenburg, C.; Winkelaar, D.; van der Hooft, E. *DOWEC 6 MW PRE-DESIGN Aero-Elastic Modelling of the DOWEC 6 MWpre-Design in PHATAS*; Technical Report; Energy research Centre of the Netherlands: Petten, The Netherlands, 2003.
49. Frost, W.; Long, B.H.; Turner, R.E. *Engineering Handbook on the Atmospheric Environmental Guidelines for Use in Wind Turbine Generator Development*; National Aeronautics and Space Administration (NASA): Washington, DC, USA, 1978.
50. Lackner, M.A.; Rotea, M.A. Passive structural control of offshore wind turbines. *Wind Energy* **2011**, *14*, 373–388. [[CrossRef](#)]
51. Den Hartog, J.P. *Mechanical Vibrations*; Dover: Garden City, NY, USA 1985; p. 342.
52. Bäumer, R.; Wollnack, S.; Scheller, J.; Starossek, U.; Werner, H. Twin rotor damper applied to the damping of non-harmonic vibrations. In Proceedings of the International Conference on Structural Dynamic, EUROODYN, Porto, Portugal, 30 June–2 July 2014; Volume 2014, pp. 1655–1661.